J. Fluid Mech. (2021), *vol*. 911, R3, doi:10.1017/jfm.2020.1130

Near-inertial parametric subharmonic instability of internal wave beams in a background mean flow

Boyu Fan[1] **and T.R. Akylas**[1],†

[1]Department of Mechanical Engineering, Massachusetts Institute of Technology, Cambridge, MA 02139, USA

(Received 7 October 2020; revised 27 November 2020; accepted 14 December 2020)

The effect of a small background constant horizontal mean flow on the parametric subharmonic instability (PSI) of locally confined internal wave beams is discussed for the case where the beam frequency is close to twice the inertial frequency due to background rotation. Under this condition, PSI is particularly potent because of the vanishing of the group velocity at the inertial frequency, which prolongs contact of near-inertial subharmonic perturbations with the primary wave. The mean flow generally stabilizes the very short-scale limit of such perturbations. By contrast, the stability of longer-scale perturbations hinges on the strength and the direction of the mean flow; particularly, a negative mean flow (antiparallel to the horizontal projection of the beam group velocity) can extend the sub-inertial range of PSI. However, a large enough mean flow of either sign ultimately weakens PSI.

Key words: internal waves

1. Introduction

In its simplest form, the parametric subharmonic instability (PSI) of internal gravity waves in stratified fluids involves the transfer of energy from a sinusoidal primary wavetrain of frequency ω_0 to two subharmonic sinusoidal perturbations via a weakly nonlinear resonant triad interaction (Staquet & Sommeria 2002). For nearly inviscid flows, the most unstable perturbations have frequency $\omega_0/2$ and short wavelength relative to the primary wave. Therefore, PSI has been suggested as a potential pathway by which internal waves transfer their energy into smaller scales and eventually dissipate in oceans (e.g. Hibiya, Nagasawa & Niwa 2002; MacKinnon & Winters 2005; Young, Tsang & Balmforth 2008). However, this proposed mechanism assumes that PSI remains robust under realistic ocean conditions (Alford *et al.* 2007; Hazewinkel & Winters 2011; MacKinnon *et al.* 2013; Sutherland 2013),

† Email address for correspondence: trakylas@mit.edu

which may not necessarily be the case considering that oceanic internal waves are far from sinusoidal.

In an effort to address this issue, recent research activity on PSI of internal waves turned to time-harmonic plane waves with locally confined, rather than sinusoidal, spatial profile (see Dauxois *et al.* (2018) for a review). Such wave beams arise in oceans from the interaction of the barotropic tide with bottom topography (e.g. Lamb 2004; Peacock, Echeverri & Balmforth 2008; Johnston *et al.* 2011). Importantly, the finite width of a beam limits the contact of short-scale subharmonic perturbations with the underlying primary wave and thus generally weakens the PSI, as the perturbations travel with the corresponding group velocity and eventually leave the beam region. As a result, PSI is only possible if either (i) the beam has nearly monochromatic profile and is sufficiently wide to allow subharmonic perturbations to stay in contact with the beam for a long enough time (Bourget *et al.* 2014; Karimi & Akylas 2014), or (ii) the beam has general locally confined profile but has frequency $\omega_0 \approx 2f$, where f is the Coriolis frequency (Karimi & Akylas 2017). In the latter case, which is directly relevant to oceans due to the Earth's rotation, subharmonic perturbations have near-inertial frequency ($\omega_0/2 \approx f$); hence, their group velocity is close to zero, which prolongs contact with the primary beam and enables PSI of beams with general profile. Furthermore, the PSI growth rates predicted by approximate theoretical models (Karimi & Akylas 2014, 2017) under the conditions (i) or (ii) above are in excellent quantitative agreement with formal linear stability analysis based on Floquet theory, provided the model also accounts for the induced perturbation components at $3\omega_0/2$ (Fan & Akylas 2020).

Another factor that may impact PSI of oceanic internal waves are large-scale currents. Numerical simulations (Richet, Muller & Chomaz 2017) of internal wave generation by tidal flow over topography near the critical latitude ($\approx 29^\circ$) where the tide frequency is equal to twice the local Coriolis parameter ($\omega_0 = 2f$) indicate that a steady background current diminishes wave dissipation by hindering the transfer of energy to smaller scales via PSI. This weakening of near-inertial PSI was attributed to the Doppler shift of the frequency of sinusoidal waves by the background current: owing to this shift, the frequency ω_0 of a sinusoidal wave moving parallel to the current can fall below $2f$, so subharmonic perturbations at $\omega_0/2$ would be sub-inertial and hence unable to propagate, preventing PSI. Later theoretical work (Fan & Akylas 2019) pointed out that a background mean flow has a more profound effect than a mere Doppler frequency shift on the PSI dynamics of a finite-width beam. Specifically, Fan & Akylas (2019) considered a nearly monochromatic beam in the absence of rotation, in which case the inertial frequency plays no role and sub-inertial perturbations are not possible; yet, the advection due to a small steady horizontal mean flow modifies the group velocity of subharmonic perturbations, which stabilizes very short-scale perturbations and can weaken PSI dramatically. This stabilizing mechanism is unique to finite-width beams, as mean flow has no effect on the PSI of a purely sinusoidal plane wave once the Doppler shift of the wave frequency has been taken into account.

As a sequel to Fan & Akylas (2019), here we discuss the effect of a small steady horizontal mean flow on the near-inertial PSI of finite-width beams with general profile. As in our earlier study, the analysis focuses on the 'distinguished limit' where advection due to the mean flow is as important as the rest of the effects that play a role in near-inertial PSI dynamics, namely, departure from inertial conditions and coupling of the perturbations with the primary wave, as well as dispersion and viscous dissipation of the perturbations. This asymptotic model leads to an eigenvalue problem that determines the PSI growth rate for a given primary wave profile under specified flow conditions. For a sinusoidal wave, as suggested by Richet *et al.* (2017), the effect of the mean flow on the PSI can be deduced

from the Doppler shift of the wave frequency, in contrast to a finite-width beam where such simplification is not possible. In the latter case, the mean flow generally stabilizes very short-scale perturbations, as was found in Fan & Akylas (2019). On the other hand, the ability of longer-scale perturbations to extract energy is controlled by the strength and the sign of the mean flow (relative to the projection of the group velocity of the beam onto the horizontal), as well as the beam frequency relative to $2f$. In particular, a mean flow antiparallel to the beam group velocity along the horizontal can extend the range of PSI to sub-inertial perturbations. However, a large enough background mean flow (e.g. comparable to the amplitude of the barotropic tide as in the simulations of Richet *et al.* (2017)) of either sign ultimately weakens PSI.

Recent related work examined, via numerical simulations (Yang *et al.* 2018) and field measurements (Yang, Wei & Zhao 2020), the effect of background geostrophic currents on PSI of an internal tide. These studies suggest that the background vorticity due to such currents shifts the Coriolis frequency and thereby affects the efficiency of PSI near the critical latitude. The present model, by contrast, considers the effect of a constant horizontal mean flow, which carries no vorticity, on the near-inertial PSI of particular disturbances, in the form of wave beams that arise as part of the internal tide (e.g. Lamb 2004; Peacock *et al.* 2008; Johnston *et al.* 2011). In this setting, our analysis shows that PSI can be impacted significantly owing to the advection of perturbations by the mean flow. As a result, the strongest PSI may be found away from the critical latitude.

2. Preliminaries

The analysis assumes an unbounded, incompressible, uniformly stratified Boussinesq fluid with constant buoyancy frequency N_* and includes the effect of background rotation, which is essential to near-inertial PSI. Using non-dimensional variables, with $1/N_*$ as the time scale and L_* as the length scale (to be specified below), the uniform horizontal background mean flow $\hat{\bar{\boldsymbol{u}}} = \bar{u}\,\hat{\boldsymbol{e}}_x$ is along x, and y is the vertical coordinate pointing antiparallel to gravity. Since PSI is a two-dimensional instability, we introduce the streamfunction $\psi(x, y, t)$, in terms of which the horizontal and vertical velocity components are ψ_y and $-\psi_x$, respectively. Thus, in a fixed reference frame, ψ, the transverse velocity $w(x, y, t)$ and the reduced density $\rho(x, y, t)$ are governed by

$$(\partial_t + \bar{u}\,\partial_x)\nabla^2\psi - \rho_x + fw_y + J(\nabla^2\psi, \psi) - \nu\nabla^4\psi = 0, \tag{2.1a}$$

$$(\partial_t + \bar{u}\,\partial_x)w - f\psi_y + J(w, \psi) - \nu\nabla^2 w = 0, \tag{2.1b}$$

$$(\partial_t + \bar{u}\,\partial_x)\rho + \psi_x + J(\rho, \psi) = 0, \tag{2.1c}$$

where $J(a, b) = a_x b_y - a_y b_x$ stands for the Jacobian. Here, f is the local Coriolis parameter (scaled by N_*) under the f-plane approximation, and $\nu = \nu_*/(N_* L_*^2)$ is the inverse Reynolds number where ν_* is the fluid kinematic viscosity.

In the inviscid limit ($\nu = 0$), the frequency ω_0 and wavevector $\boldsymbol{k}$ of infinitesimal (linear) sinusoidal plane-wave solutions of (2.1) satisfy

$$(\omega_0 - \bar{u}\,|\boldsymbol{k}|\sin\theta)^2 = f^2 + (1 - f^2)\sin^2\theta, \tag{2.2}$$

where θ is the inclination of $\boldsymbol{k}$ to the vertical. As expected, the sole effect of the background mean flow is the Doppler shift of the wave frequency on the left-hand side of (2.2). In the absence of mean flow ($\bar{u} = 0$), (2.2) reduces to the well-known internal wave dispersion relation, according to which ω_0 depends on the inclination but not on the magnitude of $\boldsymbol{k}$.

Thus, by superposing sinusoidal plane waves with the same frequency ω_0 but varying $|\boldsymbol{k}|$, it is possible to construct wave beams

$$\left.\begin{aligned} \psi_0 = Q(\eta)\,\mathrm{e}^{-\mathrm{i}\omega_0 t} + \text{c.c.}, \quad w_0 = \mathrm{i}\frac{f\cos\theta}{\omega_0} Q_\eta\,\mathrm{e}^{-\mathrm{i}\omega_0 t} + \text{c.c.}, \\ \rho_0 = -\mathrm{i}\frac{\sin\theta}{\omega_0} Q_\eta\,\mathrm{e}^{-\mathrm{i}\omega_0 t} + \text{c.c.} \end{aligned}\right\} \tag{2.3a–c}$$

that stretch along $\xi = x\cos\theta - y\sin\theta$, where the beam inclination θ to the horizontal is related to the beam frequency ω_0 via (2.2). Here, the complex amplitude $Q(\eta)$ describes the beam profile (related to the wave source) in the cross-beam direction $\eta = x\sin\theta + y\cos\theta$. Such infinitely long uniform beams happen to be also exact nonlinear states (Tabaei & Akylas 2003) and form the basis of the analyses of Karimi & Akylas (2017) and Fan & Akylas (2020) of near-inertial PSI in the absence of mean flow.

On the other hand, for $\bar{u} \neq 0$, it is clear from (2.2) that uniform beams are no longer possible, and the steady-state response to a locally confined time-harmonic wave source with frequency ω_0 will vary not only in η but also in ξ (figure 1*a*). To prevent this dispersive effect of the mean flow from altering the beam identity entirely, and also to permit analytical treatment of PSI, we assume that the mean flow is weak,

$$\bar{u} \to \mu\bar{u}, \tag{2.4}$$

where $0 < \mu \ll 1$ is a small parameter. In this instance, the length scale of ξ variations due to the mean flow is much longer than a characteristic beam width, which is chosen as the length scale L_*. Specifically, taking $\boldsymbol{k} = k_1\hat{\boldsymbol{e}}_\eta + k_2\hat{\boldsymbol{e}}_\xi$ with $k_2 \ll k_1 = O(1)$, it follows from (2.2) that

$$\omega_0 = \Omega_0 + \frac{(1-f^2)\sin\theta\cos\theta}{\Omega_0}\frac{k_2}{k_1} + \mu\bar{u}\sin\theta\, k_1 + O(\mu k_2, k_2^2), \tag{2.5}$$

where $\Omega_0^2 = f^2 + (1-f^2)\sin^2\theta$, so $k_2/k_1 = O(\mu)$. Therefore, the length scale of ξ variations is $O(\mu L_*)$ and, considering that PSI involves fine-scale perturbations (relative to L_*), these variations may be neglected: at a given $\xi = \xi_0$, the beam locally appears uniform (see figure 1*b*) and (2.3*a–c*) can be used as the basic state in the ensuing stability analysis provided L_* and Q are taken at ξ_0.

Furthermore, our analysis assumes small-amplitude beams, so we write

$$Q \to \epsilon Q, \tag{2.6}$$

where $\epsilon = U_*/(N_*L_*) \ll 1$ is an amplitude parameter and U_* is a (dimensional) characteristic along-beam velocity. In addition, as our focus is on near-inertial PSI, the beam frequency ω_0 is taken to be close to $2f$:

$$\omega_0 = 2f + \sigma\delta, \tag{2.7}$$

where $0 < \delta \ll 1$ is a small parameter. Here, the frequency detuning $\sigma = O(1)$ may be either positive or negative so that subharmonic perturbations at $\omega_0/2$ may be super- or sub-inertial, respectively. The relative magnitudes of the small parameters μ, ϵ and δ introduced in (2.4), (2.6) and (2.7) are specified below.

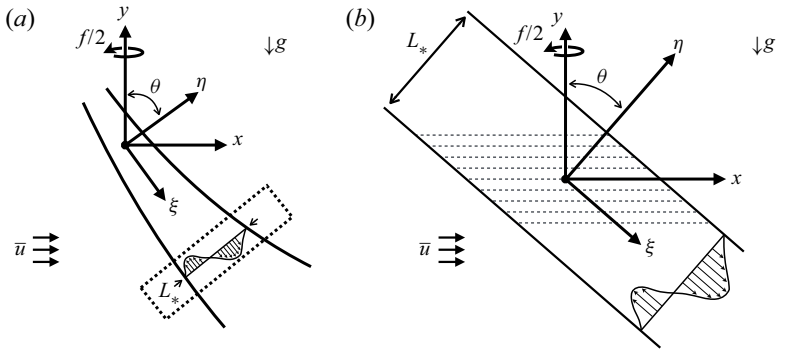

Figure 1. Schematic of the PSI geometry. (*a*) Locally confined primary wave beam of general profile with frequency ω_0 and typical (dimensional) width L_* in the presence of a small horizontal background mean flow $\bar{u}$. (*b*) Close-up view of the beam slice shown in the dotted box in (*a*). The beam geometry at any given ξ location can be assumed to be locally uniform along ξ, as ξ variations have a much longer length scale than η variations. Subharmonic perturbations of frequency $\omega_0/2 \approx f$ are fine-scale wavepackets with nearly horizontal lines of constant phase (dotted lines).

3. Near-inertial PSI model

We now specify the form of the perturbations in the stability analysis of the basic state (2.3*a–c*). From prior experience with near-inertial PSI in the absence of mean flow (Karimi & Akylas 2017; Fan & Akylas 2020), to cause instability, the subharmonic perturbations of frequency approximately $\omega_0/2$ must interact with the $O(\epsilon)$ primary wave for long enough, namely for $O(\epsilon^{-1})$ wave periods. Thus, nonlinear coupling with the underlying beam sets the 'slow' time $T = \epsilon t$, and all other effects that have a part in PSI dynamics, including the background mean flow, are scaled in accordance with this fundamental-to-PSI time scale. Specifically, the perturbation comprises two fine-scale subharmonic wavepackets with $O(\epsilon^{-1/2})$ carrier wavenumber so that dispersion comes in to play when $T = O(1)$. Furthermore, wave dispersion is made as important as the frequency detuning (2.7), which controls the small group velocity of the two wavepackets at near-inertial conditions, and the small viscosity (measured by the inverse Reynolds number ν) via the scalings

$$\delta = \epsilon, \quad \nu = \alpha\epsilon^2, \tag{3.1a,b}$$

where α is an $O(1)$ viscous parameter. Finally, the advection of the perturbation wavepackets due to the small mean flow (2.4) is incorporated into this 'distinguished limit' by setting

$$\mu = \epsilon. \tag{3.2}$$

Following these scaling considerations, infinitesimal perturbations $(\tilde{\psi}, \tilde{w}, \tilde{\rho})$ to the primary wave beam (ψ_0, w_0, ρ_0) in (2.3*a–c*) are taken in the form

$$\tilde{\psi} = \frac{\epsilon^{1/2}}{\kappa}\{[A\exp(\mathrm{i}\kappa y/\epsilon^{1/2}) + B\exp(-\mathrm{i}\kappa y/\epsilon^{1/2})]\exp(-\mathrm{i}\omega_0 t/2) + \text{c.c.}\}$$
$$+ \frac{\epsilon}{\kappa}\{[A_3\exp(\mathrm{i}\kappa y/\epsilon^{1/2}) + B_3\exp(-\mathrm{i}\kappa y/\epsilon^{1/2})]\exp(-\mathrm{i}3\omega_0 t/2) + \text{c.c.}\}, \tag{3.3a}$$

$$\tilde{w} = \{[M\exp(\mathrm{i}\kappa y/\epsilon^{1/2}) + N\exp(-\mathrm{i}\kappa y/\epsilon^{1/2})]\exp(-\mathrm{i}\omega_0 t/2) + \text{c.c.}\}$$
$$+ \epsilon^{1/2}\{[M_3\exp(\mathrm{i}\kappa y/\epsilon^{1/2}) + N_3\exp(-\mathrm{i}\kappa y/\epsilon^{1/2})]\exp(-\mathrm{i}3\omega_0 t/2) + \text{c.c.}\}, \quad (3.3b)$$

$$\tilde{\rho} = \epsilon^{1/2}\{[F\exp(\mathrm{i}\kappa y/\epsilon^{1/2}) + G\exp(-\mathrm{i}\kappa y/\epsilon^{1/2})]\exp(-\mathrm{i}\omega_0 t/2) + \text{c.c.}\}, \quad (3.3c)$$

where the complex amplitudes A, B, A_3, B_3, M, N, M_3, N_3, F and G are functions of (ξ, η, T). The leading-order terms in (3.3) are subharmonic perturbations at $\omega_0/2 \approx f$ (cf. (2.7)) that comprise two fine-scale wavepackets with $O(\epsilon^{-1/2})$ carrier wavenumber, as discussed above. In keeping with (2.2) for small mean flow, the carrier wavevectors of these near-inertial wavepackets are along the vertical (figure 1*b*) and also have equal magnitude but opposite sign; thus, to leading order, the subharmonic perturbations form a resonant triad with the primary wave. Furthermore, $\tilde{\psi}$ and $\tilde{w}$ in (3.3*a*) and (3.3*b*) include disturbances with frequency $3\omega_0/2$. These components have the same fine-scale structure as those at $\omega_0/2$, but smaller amplitude, and arise from the interaction of the subharmonic perturbations with the primary wave ($\tilde{\rho}$ features similar $3\omega_0/2$ components, but these are not displayed in (3.3*c*) as they do not affect the perturbation dynamics at leading order). As pointed out in Fan & Akylas (2020), the perturbations at $3\omega_0/2$ play an important part in PSI dynamics and were erroneously omitted in earlier analyses (e.g. Karimi & Akylas 2017). Finally, the parameter $\kappa = O(1)$, taken to be positive without loss of generality, controls the vertical wavenumber of the perturbation wavepackets and will be used to determine the maximum PSI growth rate.

Inserting (3.3) into (2.1) after linearizing with respect to the perturbations, and collecting the various harmonics, we first solve for the amplitudes of the $3\omega_0/2$ waves:

$$A_3 = -M_3 = -\frac{\kappa\sin\theta}{2f}AQ_\eta, \quad B_3 = N_3 = \frac{\kappa\sin\theta}{2f}BQ_\eta. \quad (3.4a,b)$$

Next, upon eliminating F, G, M and N, and making use of (3.4*a*,*b*), we obtain the following coupled evolution equations for the subharmonic wave envelopes A and B:

$$A_T - \mathrm{i}\frac{\sigma}{2}A + \bar{u}\sin\theta\, A_\eta - \mathrm{i}\frac{c'}{2\kappa^2}A_{\eta\eta} + \alpha\kappa^2 A + \gamma Q_{\eta\eta}B^* = 0, \quad (3.5a)$$

$$B_T - \mathrm{i}\frac{\sigma}{2}B + \bar{u}\sin\theta\, B_\eta - \mathrm{i}\frac{c'}{2\kappa^2}B_{\eta\eta} + \alpha\kappa^2 B + \gamma Q_{\eta\eta}A^* = 0, \quad (3.5b)$$

where

$$c' = 3f, \quad \gamma = \tfrac{3}{4}\sin\theta\cos\theta. \quad (3.6a,b)$$

The second term of (3.5) corresponds to the effect of inertial frequency detuning, the third to the effect of the mean flow, the fourth to dispersion, the fifth to viscous dissipation and the sixth to the coupling of the subharmonic perturbations with the underlying wave. Based on (3.5), the leading-order effect of the mean flow is to advect the subharmonic wavepackets, similar to the PSI of nearly monochromatic beams in a weak background mean flow (Fan & Akylas 2019). Finally, it should be noted that, even though we have allowed for general $O(1)$ variations in the perturbation envelopes in (3.3), the final stability equations (3.5) involve derivatives with η only, indicating that ξ variations have no effect on the stability to leading order.

4. Stability eigenvalue problem

The evolution equations (3.5) of infinitesimal near-inertial perturbations depend on the beam profile $Q(\eta)$, as well as the independent parameters $(f, \sigma, \bar{u}, \alpha, \kappa)$. Although (3.5)

can be readily solved numerically, a comprehensive study across all values of these five parameters is formidable. Therefore, in the following we focus on the case

$$f \ll 1, \tag{4.1}$$

an approximation that is well justified for oceanic internal waves where typically $f \lesssim 0.1$. In this limit, we may eliminate f from (3.5) by the rescaling

$$T \to T/f, \quad \sigma \to f\sigma, \quad \alpha \to f\alpha \tag{4.2a–c}$$

and using the leading-order expressions for $\sin\theta = \sqrt{3}f$ and $\gamma = 3\sqrt{3}f/4$, obtained via (2.2), (2.4), (2.7) and (4.2*a–c*). In addition, to examine the stability of the primary wave, we look for solutions in the form of normal modes,

$$(A, B^*) = (a, b^*)\,\mathrm{e}^{\lambda T}, \tag{4.3}$$

where $\lambda = \lambda_r + \mathrm{i}\lambda_i$ and $\lambda_r > 0$ implies instability. Thus, making use of (4.1)–(4.3), equations (3.5) reduce to

$$\left(\hat{\lambda} - \mathrm{i}\frac{\sigma}{2}\right) a + \bar{u}\sqrt{3}\, a_\eta - \mathrm{i}\frac{3}{2\kappa^2} a_{\eta\eta} + \frac{3\sqrt{3}}{4} Q_{\eta\eta} b^* = 0, \tag{4.4a}$$

$$\left(\hat{\lambda} + \mathrm{i}\frac{\sigma}{2}\right) b^* + \bar{u}\sqrt{3}\, b^*_\eta + \mathrm{i}\frac{3}{2\kappa^2} b^*_{\eta\eta} + \frac{3\sqrt{3}}{4} Q^*_{\eta\eta} a = 0, \tag{4.4b}$$

where

$$\hat{\lambda} = \lambda + \alpha\kappa^2. \tag{4.5}$$

For a given primary wave profile $Q(\eta)$, frequency detuning σ and mean flow $\bar{u}$, the equation system (4.4) along with suitable boundary conditions, as discussed below, define an eigenvalue problem for $\hat{\lambda} = \hat{\lambda}_r + \mathrm{i}\hat{\lambda}_i$. In view of (4.5), instability arises if $\hat{\lambda}_r(\kappa) > \alpha\kappa^2$. Thus, $\hat{\lambda}_r$ corresponds to the inviscid growth rate, whereas the actual growth rate λ_r takes into account the effect of viscous dissipation ($\alpha > 0$).

Finally, as expected on intuitive grounds, upon the substitution $Q(\eta) \to Q(-\eta)$ (which reverses the direction in which a wave beam transports energy), it follows from (4.4) that the same stability results hold if the mean flow also is reversed, $\bar{u} \to -\bar{u}$.

5. Sinusoidal plane wave

First, we examine the PSI of

$$Q = \tfrac{1}{2}\mathrm{e}^{\mathrm{i}\eta}, \tag{5.1}$$

which corresponds to a uniform sinusoidal plane wave with non-dimensional peak amplitude ϵ and dimensional wavelength $2\pi L_*$. For this primary wave profile, eigenmode

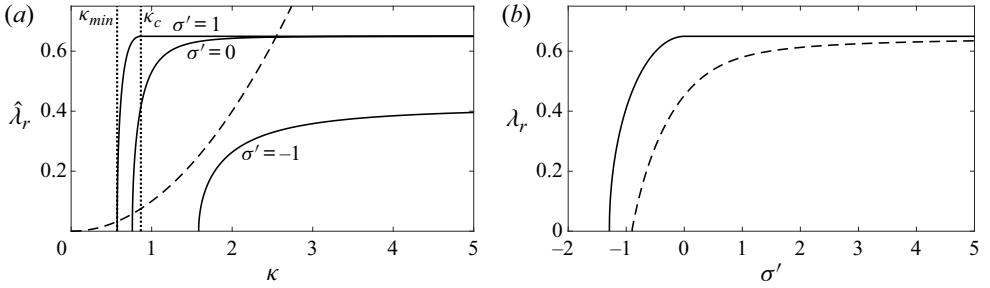

Figure 2. Predictions of the characteristic equation (5.3) for the PSI of a sinusoidal plane wave. (*a*) Inviscid growth rate $\hat{\lambda}_r$ as a function of the perturbation wavenumber parameter κ for various values of the inertial detuning σ' (labelled). Vertical dotted lines correspond to κ_{min} and κ_c (labelled) for $\sigma' = 1$. The dashed line plots the quadratic $\alpha\kappa^2$ for $\alpha = 0.1$ that controls viscous dissipation. (*b*) Maximum PSI growth rate λ_r, taken over all κ, as a function of σ' for $\alpha = 0$ (solid line) and $\alpha = 0.1$ (dashed line), corresponding to inviscid and viscous flow conditions, respectively.

solutions of (4.4) satisfy periodic boundary conditions in η and take the form

$$(a, b^*) = (a_0\, \mathrm{e}^{\mathrm{i}\eta/2}, b_0^*\, \mathrm{e}^{-\mathrm{i}\eta/2})\mathrm{e}^{\mathrm{i}\rho\eta}, \tag{5.2}$$

where ρ is a real wavenumber parameter. Upon substituting (5.1) and (5.2) into (4.4), we obtain a characteristic equation that can be readily solved for λ:

$$\lambda = \frac{3}{8}\sqrt{3 - \mathbb{C}^2} - \alpha\kappa^2 - \mathrm{i}\left(\frac{3}{2\kappa^2} + \bar{u}\sqrt{3}\right)\rho \tag{5.3}$$

with

$$\mathbb{C} = \left(\frac{4}{3}\sigma' - \frac{1}{\kappa^2}\right) - \frac{4\rho^2}{\kappa^2}, \quad \sigma' = \sigma - \bar{u}\sqrt{3}. \tag{5.4a,b}$$

Here, the effect of the mean flow $\bar{u}$ appears together with the frequency detuning σ in the form of the parameter σ', which can be interpreted as the frequency detuning in the reference frame of the fluid moving with the background mean flow. Indeed, according to (2.2), (2.7), (3.1*a*,*b*) and (4.2*a*–*c*), the primary wave in the reference frame of the fluid has frequency $\omega_0 - \epsilon\bar{u}\sin\theta = 2f(1 + \epsilon\sigma'/2)$. This confirms that a constant, uniform, background mean flow has no effect on the PSI of a sinusoidal plane wave once the Doppler shift of the primary wave frequency is taken into account.

Based on (5.3), and noting that $\mathbb{C}$ in (5.4*a*,*b*) is a monotonically increasing function of $\kappa > 0$, a necessary condition for PSI is that $\mathbb{C} > -\sqrt{3}$, or equivalently $\kappa > \kappa_{\min} = \sqrt{3/(4\sigma' + 3\sqrt{3})}$ (see figure 2*a*). This implies that PSI is only possible for $\sigma' > -3\sqrt{3}/4$, which indicates that slightly sub-inertial perturbations (in the reference frame of the fluid) can be unstable (see figure 2*b*).

In the inviscid limit ($\alpha = 0$), examined earlier in Young *et al.* (2008), the maximum growth rate $\lambda_r = 3\sqrt{3}/8$ is obtained when $\mathbb{C} = 0$, which is always possible for a suitable choice of ρ if the quantity in the parentheses in (5.4*a*,*b*) is positive, or equivalently $\kappa \geqslant \kappa_c = \sqrt{3/(4\sigma')}$ (see figure 2*a*). Therefore, super-inertial PSI ($\sigma' > 0$) is universal for any $\kappa \geqslant \kappa_c$ with no scale selection. On the other hand, for $\sigma' \leqslant 0$, the maximum growth rate requires $\kappa \to \infty$. These results are in agreement with Young *et al.* (2008).

Under viscous flow conditions ($\alpha > 0$), high-wavenumber ($\kappa \gg 1$) modes are stabilized because the quadratic $\alpha\kappa^2$ in (5.3) will always exceed the inviscid growth rate. As a result,

no instability is possible for $\kappa > \sqrt{3\sqrt{3}/(8\alpha)}$. Furthermore, in the super-inertial range $\sigma' > 0$, the PSI growth rate monotonically decreases for $\kappa \geqslant \kappa_c$ owing to the increased effect of viscous dissipation, so the maximum PSI growth rate can always be found in the range $\kappa_{\min} < \kappa \leqslant \kappa_c$.

6. Locally confined beam

We now examine the effect of mean flow on PSI of a locally confined beam ($Q \to 0$ as $\eta \to \pm\infty$). Here, eigenmode solutions of (4.4) decay far from the beam:

$$(a, b^*) \to 0 \quad (\eta \to \pm\infty). \tag{6.1}$$

Specifically, we consider the Gaussian beam profile

$$Q = \frac{1}{\sqrt{8\pi}} \int_0^\infty \mathrm{e}^{-l^2/8}\, \mathrm{e}^{\mathrm{i}l\eta}\, \mathrm{d}l, \tag{6.2}$$

which comprises sinusoidal plane waves with positive wavenumber ($l > 0$) and therefore represents a unidirectional, progressive wave beam (Tabaei & Akylas 2003) that transports energy in the positive ξ direction (see figure 1). The equation system (4.4) subject to (6.1) is discretized using eighth-order centred finite differences and the resulting matrix eigenvalue problem for $\hat{\lambda}(\kappa; \sigma, \bar{u})$ is solved using standard eigenvalue packages in MATLAB. Typically, we used the grid spacing $\Delta\eta = 0.05$ and the domain $\eta \in [-50, 50]$, although these values were varied somewhat depending on the parameters σ and $\bar{u}$.

Figure 3(a) plots the real part of $\hat{\lambda} = \hat{\lambda}_r + \mathrm{i}\hat{\lambda}_i$ (i.e. the inviscid growth rate) as a function of the wavenumber parameter κ, exactly at inertial conditions ($\sigma = 0$), for the representative values of mean flow $\bar{u} = 0$, 0.5 and -1. Furthermore, the quadratic $\alpha\kappa^2$ that controls the effect of viscosity in view of (4.5) is shown for $\alpha = 0.1$. Overall, we find that $\bar{u} \neq 0$ has a strong stabilizing effect on perturbations with large κ, even in the absence of viscosity: while the maximum inviscid growth rate for $\bar{u} = 0$ is found as $\kappa \to \infty$ (i.e. extremely fine-scale perturbations), in the case of $\bar{u} = 0.5$ and -1 instability is confined to $\kappa \lesssim 5$. This stabilizing effect of mean flow irrespective of the sign of $\bar{u}$ on very fine-scale perturbations is analogous to the results of Fan & Akylas (2019) for beams in the absence of background rotation, and suggests that PSI is less effective as a pathway to small-scale mixing in the presence of mean flow. It should be noted that stabilization of large-κ disturbances due to mean flow does not occur for a plane sinusoidal wave, as the range of maximum inviscid PSI extends to $\kappa \to \infty$ (figure 2a).

Figure 3(a) also indicates that, unlike very short-scale ($\kappa \gg 1$) perturbations, which are stabilized by mean flow of either sign, the stability of (longer-scale) disturbances with $\kappa = O(1)$ depends crucially on the sign of $\bar{u}$. Specifically, as illustrated by $\bar{u} = 0.5$, $\bar{u} > 0$, in which case the mean flow is parallel to the projection of the group velocity of the beam onto the horizontal, has a strong stabilizing effect on PSI for all κ. By contrast, for $\bar{u} = -1$, there is a small range of κ ($0.5 \lesssim \kappa \lesssim 2.5$) where the presence of negative mean flow enhances instability relative to no mean flow. Furthermore, this range includes the disturbance with the maximum inviscid growth rate, found at $\kappa \approx 1.6$.

These perhaps unexpected results can be understood by examining the dominant instability eigenvalues $\hat{\lambda} = \hat{\lambda}_r + \mathrm{i}\hat{\lambda}_i$ and corresponding eigenmodes $a(\eta)$ and $b(\eta)$ as $\bar{u}$ is varied. Starting with $\bar{u} = 0$, near-inertial PSI is controlled by two distinct types of instability modes, one having complex ($\hat{\lambda}_i \neq 0$) and the other purely real ($\hat{\lambda}_i = 0$) eigenvalues. The associated eigenmodes are locally confined in the vicinity of the

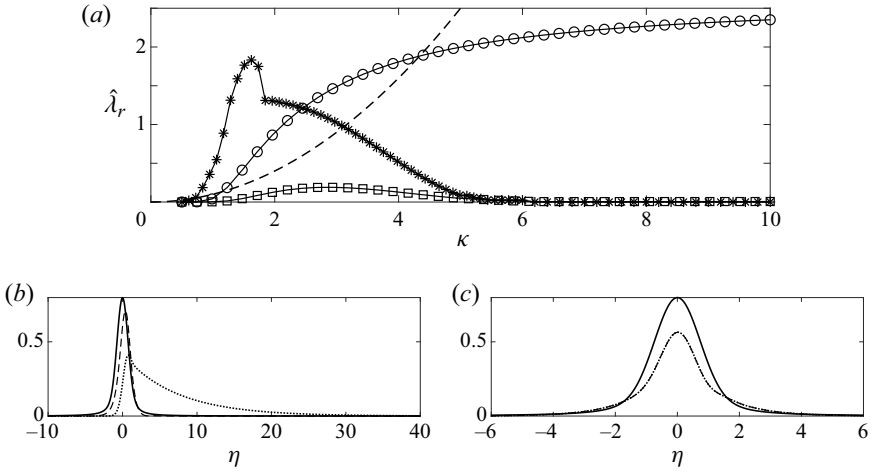

Figure 3. (*a*) Inviscid PSI growth rate $\hat{\lambda}_r$, for the beam profile (6.2) as a function of the perturbation wavenumber parameter κ at inertial conditions ($\sigma = 0$) and for mean flow $\bar{u} = 0$ (○), 0.5 (□) and -1 (∗). The dashed line plots the quadratic $\alpha\kappa^2$ for $\alpha = 0.1$ that controls viscous dissipation. (*b*) Perturbation wavepacket envelope magnitudes $|a|$ (dashed line) and $|b|$ (dotted line) corresponding to the highest inviscid growth rate for $\bar{u} = 0.5$, found at $\kappa \approx 2.9$, in panel (*a*). Here $\sqrt{|a|^2 + |b|^2}$ is normalized to have the same maximum value as the primary wave along-beam velocity $|Q_\eta|$ (solid line). (*c*) Same as (*b*) but for the maximum inviscid growth rate for $\bar{u} = -1$, found at $\kappa \approx 1.6$, in panel (*a*). In this case, $|a| = |b|$.

underlying wave beam. The first of these two eigensolution branches provides the dominant instability (highest growth rate $\hat{\lambda}_r$) when $\sigma \geqslant 0$ (super-inertial PSI range), while the second prevails when $\sigma < 0$ (sub-inertial PSI range), for all κ. Turning on $\bar{u}$, these two types of modes continue to coexist. However, which one is dominant is now decided not only by σ but also by the strength and sign of $\bar{u}$, as well as κ. Key to this mode competition is the fact that the mean flow advects the eigenmodes of the first eigensolution branch outside the beam region, limiting their ability to extract energy from the beam. This advection effect is illustrated in figure 3(*b*), which plots the eigenmode corresponding to the highest inviscid growth rate for $\bar{u} = 0.5$ at $\kappa \approx 2.9$ in figure 3(*a*). It should be noted that $|b|$ extends far outside the region of the primary beam. Moreover, all instability growth rates for $\bar{u} = 0.5$ in figure 3(*a*) correspond to such advected modes, which explains the overall stabilizing effect of mean flow for $\bar{u} > 0$. On the other hand, under the condition $\hat{\lambda}_i = 0$, it follows from (4.4) that $a(\eta) = b(\eta)$ so the modes of the second eigenvalue branch correspond to standing waves in the vertical (cf. (3.3) and (4.3)).

Furthermore, these modes can remain fully confined to the vicinity of the primary beam in the presence of mean flow, as illustrated in figure 3(*c*) for the eigenmode corresponding to the highest inviscid growth rate for $\bar{u} = -1$ at $\kappa \approx 1.6$ in figure 3(*a*). In this instance, the dominant eigenvalues for $1 \lesssim \kappa \lesssim 1.9$ correspond to fully confined standing wave modes with $\hat{\lambda}_i = 0$ similar to that shown in figure 3(*c*), whereas those for $\kappa \gtrsim 1.9$ (and $\kappa \lesssim 1$) correspond to advected modes similar to that in figure 3(*b*), but extending far from the beam in $\eta \ll -1$ as expected for $\bar{u} < 0$ (the kink in the plot of $\hat{\lambda}_r$ for $\bar{u} = -1$ at $\kappa \approx 1.9$ in figure 3(*a*) is due to the transition between these two different eigenvalue branches). Therefore, the enhancement of instability for $\bar{u} = -1$ in figure 3(*a*) is attributed to the emergence of strongly 'trapped' standing wave modes in $1 \lesssim \kappa \lesssim 1.9$, which allow for efficient energy extraction from the primary beam. This mode trapping becomes possible owing to the counterbalancing of the mean-flow advection terms by the dispersion terms

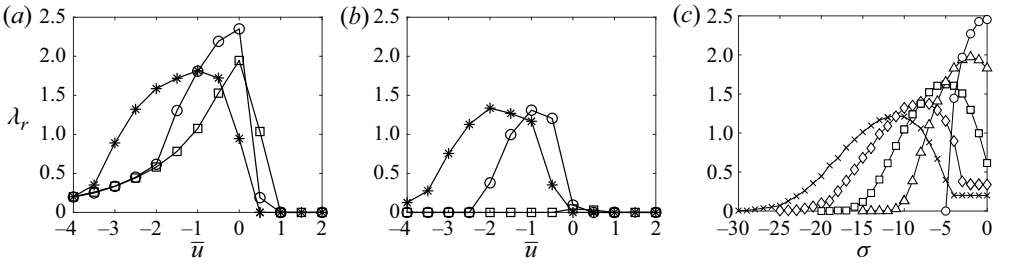

Figure 4. (*a*) Maximum PSI growth rate λ_r for the locally confined beam profile (6.2) under inviscid flow conditions ($\alpha = 0$) as a function of mean flow $\bar{u}$ for frequency detuning $\sigma = -4$ (∗), 0 (○) and 10 (□). (*b*) Same as (*a*) but for $\alpha = 0.2$. (*c*) Maximum inviscid ($\alpha = 0$) PSI growth rate as a function of $\sigma \leqslant 0$ for $\bar{u} = 0$ (○), -1 (△), -2 (□), -3 (◇) and -4 (×).

in the evolution equations (3.5). Such modes play an important role in PSI for $\bar{u} < 0$ and $\sigma \leqslant 0$ in general, as discussed below.

Figure 4(*a*) plots the maximum inviscid PSI growth rates, taken over κ, as a function of the mean flow $-4 \leqslant \bar{u} \leqslant 2$ for inertial detuning parameter $\sigma = -4$, 0 and 10. Overall, the PSI is almost entirely stabilized for $\bar{u} \gtrsim 1$ and for $\bar{u} \lesssim -4$, indicating that a large enough mean flow of either sign eventually weakens the PSI. Importantly, however, for $\sigma = -4$, corresponding to sub-inertial subharmonic perturbations ($\omega_0/2 < f$), PSI growth rates actually are increased by the presence of small negative mean flow (reaching a maximum at $\bar{u} \approx -1$). This enhancement of instability is due to the confinement of the perturbation close to the beam for $\sigma \leqslant 0$ and $\bar{u} < 0$ noted earlier (figure 3*c*), which allows energy to be extracted from the beam more efficiently than for $\sigma > 0$ or $\bar{u} > 0$.

Furthermore, such 'trapped' modes typically occur for relatively small perturbation wavenumber κ (e.g. figure 3*a*), so they are less susceptible to the stabilizing effects of viscous dissipation. As a result, for large enough viscosity (e.g. $\alpha = 0.2$ as shown in figure 4*b*), PSI growth rates for sub-inertial perturbations ($\sigma = -4$) and $\bar{u} < 0$ can even exceed those at inertial conditions ($\sigma = 0$). It should be noted that the kink in figure 4(*a*) at $\bar{u} = -2$ for $\sigma = 0$ corresponds to a transition between different eigenvalue branches, in a similar fashion to the kink at $\kappa \approx 1.9$ in figure 3(*a*). Finally, figure 4(*c*) plots the maximum inviscid PSI growth rate, taken over κ, as a function of $-30 \leqslant \sigma \leqslant 0$ for $-4 \leqslant \bar{u} \leqslant 0$. These results indicate that negative mean flow also extends the range of PSI to primary wave frequencies well below $\omega_0 = 2f$. This effect is reminiscent of the near-inertial PSI of a plane wave in the presence of mean flow (see § 5), where instability only depends on the combined parameter $\sigma' = \sigma - \bar{u}\sqrt{3}$ (cf. (5.4*a*,*b*)) and may therefore occur for any arbitrary σ, provided a suitable $\bar{u}$. However, the present asymptotic theory assumes $|\sigma| = O(1)$ and thus may not be strictly valid for $|\sigma| \gg 1$.

7. Concluding remarks

We developed a theoretical model for near-inertial PSI of general finite-width beams in the presence of a small background constant horizontal mean flow. As in the case of nearly monochromatic beams and no background rotation (Fan & Akylas 2019), the mean flow advects subharmonic perturbations and generally has a stabilizing effect on the very short-scale disturbance limit of PSI. Here, however, an additional factor that plays an important part in the stability of longer-scale perturbations is the mean flow direction: a mean flow parallel to the horizontal projection of the beam group velocity is always stabilizing, whereas a suitable small amount of mean flow in the opposite direction can

strengthen PSI and extend the range of instability to sub-inertial perturbations. Thus, as also noted by Richet *et al.* (2017) and Yang *et al.* (2018), the strongest PSI may be found away from the critical frequency $\omega_0 = 2f$, depending on the mean flow. Based on our results, $\bar{u} = O(1)$ is sufficient to impact PSI significantly. Using $N_* = 10^{-3}$ s^{-1} as in Richet *et al.* (2017) and for beam width $L_* = 500$ m and amplitude parameter $\epsilon = 0.1$, $\bar{u} = O(1)$ translates to a dimensional mean flow of $O(5$ cm s$^{-1})$, in the same ballpark as 2.5 cm s^{-1} used in these simulations.

Funding. This work was supported in part by the US National Science Foundation under grant DMS-1512925 and a Graduate Research Fellowship (grant 1122374) to B.F.

Declaration of interests. The authors report no conflict of interest.

Author ORCIDs.
Boyu Fan https://orcid.org/0000-0002-1743-5225.

References

Alford, M.H., MacKinnon, J.A., Zhao, Z., Pinkel, R., Klymak, J. & Peacock, T. 2007 Internal waves across the pacific. *Geophys. Res. Lett.* **34** (24), L24601.

Bourget, B., Scolan, H., Dauxois, T., Le Bars, M., Odier, P. & Joubaud, S. 2014 Finite-size effects in parametric subharmonic instability. *J. Fluid Mech.* **759**, 739–750.

Dauxois, T., Joubaud, S., Odier, P. & Venaille, A. 2018 Instabilities of internal gravity wave beams. *Annu. Rev. Fluid Mech.* **50** (1), 131–156.

Fan, B. & Akylas, T.R. 2019 Effect of background mean flow on PSI of internal wave beams. *J. Fluid Mech.* **869**, R1.

Fan, B. & Akylas, T.R. 2020 Instabilities of finite-width internal wave beams: from Floquet analysis to PSI. *J. Fluid Mech.* (in press).

Hazewinkel, J. & Winters, K.B. 2011 PSI of the internal tide on a β plane: flux divergence and near-inertial wave propagation. *J. Phys. Oceanogr.* **41** (9), 1673–1682.

Hibiya, T., Nagasawa, M. & Niwa, Y. 2002 Nonlinear energy transfer within the oceanic internal wave spectrum at mid and high latitudes. *J. Geophys. Res. Oceans* **107** (C11), 3207.

Johnston, T.M.S., Rudnick, D.L., Carter, G.S., Todd, R.E. & Cole, S.T. 2011 Internal tidal beams and mixing near monterey bay. *J. Geophys. Res.* **116**, C03017.

Karimi, H.H. & Akylas, T.R. 2014 Parametric subharmonic instability of internal waves: locally confined beams versus monochromatic wavetrains. *J. Fluid Mech.* **757**, 381–402.

Karimi, H.H. & Akylas, T.R. 2017 Near-inertial parametric subharmonic instability of internal wave beams. *Phys. Rev. Fluids* **2** (7), 074801.

Lamb, K.G. 2004 Nonlinear interaction among internal wave beams generated by tidal flow over supercritical topography. *Geophys. Res. Lett.* **31** (9), L09313.

MacKinnon, J.A., Alford, M.H., Sun, O., Pinkel, R., Zhao, Z. & Klymak, J. 2013 Parametric subharmonic instability of the internal tide at 29°N. *J. Phys. Oceanogr.* **43** (1), 17–28.

MacKinnon, J.A. & Winters, K.B. 2005 Subtropical catastrophe: significant loss of low-mode tidal energy at 28.9°. *Geophys. Res. Lett.* **32** (15), L15605.

Peacock, T., Echeverri, P. & Balmforth, N.J. 2008 An experimental investigation of internal tide generation by two-dimensional topography. *J. Phys. Oceanogr.* **38** (1), 235–242.

Richet, O., Muller, C. & Chomaz, J.-M. 2017 Impact of a mean current on the internal tide energy dissipation at the critical latitude. *J. Phys. Oceanogr.* **47** (6), 1457–1472.

Staquet, C. & Sommeria, J. 2002 Internal gravity waves: from instabilities to turbulence. *Annu. Rev. Fluid Mech.* **34** (1), 559–593.

Sutherland, B.R. 2013 The wave instability pathway to turbulence. *J. Fluid Mech.* **724**, 1–4.

Tabaei, A. & Akylas, T.R. 2003 Nonlinear internal gravity wave beams. *J. Fluid Mech.* **482**, 141–161.

Yang, W., Hibiya, T., Tanaka, Y., Zhao, L. & Wei, H. 2018 Modification of parametric subharmonic instability in the presence of background geostrophic currents. *Geophys. Res. Lett.* **45** (23), 12957–12962.

Yang, W., Wei, H. & Zhao, L. 2020 Parametric subharmonic instability of the semidiurnal internal tides at the East China Sea shelf slope. *J. Phys. Oceanogr.* **50** (4), 907–920.

Young, W.R., Tsang, Y.-K. & Balmforth, N.J. 2008 Near-inertial parametric subharmonic instability. *J. Fluid Mech.* **607**, 25–49.